Article

Bull. Volcanol. Soc. Japan
Vol. 60 (2015) No. 1, pp. 35−46

Internal Structure of Kuttara Caldera, Hokkaido, Japan

Yoshihiko GOTO* and Akira JOHMORI**

(Received August 7, 2014; Accepted January 30, 2015)

A controlled-source audio-frequency magnetotelluric (CSAMT) survey was conducted across the caldera of Kuttara volcano, Hokkaido, Japan, to investigate its subsurface structure. The caldera is 3 km in diameter and contains a circular lake (Lake Kuttara) 2.5 km across. The CSAMT survey was conducted along a 12-km-long east–west-trending transect that crossed the volcano and passed over the caldera. A total of 23 receiver stations were distributed along the survey line, including 7 stations in the caldera. Unique on-boat measurements were obtained at the surface of Lake Kuttara. A two-dimensional inversion of the CSAMT data, which revealed the resistivity structure to depths of up to 1000 m beneath the caldera, suggested the existence of a low-resistivity region ($<30\,\Omega\cdot$m) beneath the eastern caldera floor, extending subvertically for >1000 m and with a width of 1300−1500 m. The structure is interpreted to be a region filled with lava blocks and pyroclasts, which subsided during collapse of the caldera and which has been affected by hydrothermal alteration. The location of the low-resistivity region corresponds to an oval basin in the eastern part of the lake, implying that caldera subsidence occurred mainly beneath this basin. The western part of the caldera floor tilts gently to the east and has a rugged surface, suggesting that the western caldera rim was significantly enlarged as a result of landsliding during caldera formation. We thus infer that the Kuttara caldera was produced by asymmetric caldera collapse, which is attributed to the geological heterogeneity of the Kuttara volcano, with an eastern part comprised mainly of andesitic lavas and a western part comprised mainly of dacitic pyroclastic deposits.

Key words: resistivity survey, CSAMT method, caldera, internal structure, Kuttara volcano

1. Introduction

The Kuttara caldera (3 km in diameter), Kuttara volcano, southwestern Hokkaido, Japan, is one of the smallest Quaternary calderas in Japan (Fig. 1). The caldera contains a remarkably circular freshwater lake, Lake Kuttara (Fig. 2A). Subsurface geological structures of the caldera have been previously studied by a gravity survey (Yokoyama *et al.*, 1967), but details of the structures remain poorly constrained. We conducted a controlled-source audio-frequency magnetotelluric (CSAMT) resistivity survey (Milsom, 2003; Sandberg and Hohmann, 1982) to investigate its internal structure. As the Kuttara caldera contains a lake, we obtained unique on-boat CSAMT measurements from the lake surface. A two-dimensional inversion of the CSAMT data revealed the resistivity structure at depths of up to 1000 m beneath the caldera. We here present the results of the resistivity survey, and discuss the nature of the subsurface geological structures beneath the caldera.

2. Kuttara caldera

The Kuttara caldera is located at the summit of Kuttara volcano (Fig. 2). Volcanic activity on Kuttara volcano, which occurred from 80 to 40 ka, included an early period of silicic explosive activity followed by the construction of an andesitic stratovolcano (Katsui *et al.*, 1988; Moriizumi, 1998; Moriya, 2003; Yamagata, 1994). The stratovolcano (elevation, 549 m above sea level; base diameter, 9 km) consists mainly of andesitic lavas and scoria, and associated dacitic pyroclastic deposits (Katsui *et al.*, 1988). The andesitic lavas and scoria are distributed on the northern, eastern, and southern parts of the stratovolcano, whereas the dacitic pyroclastic deposits are distributed on the western part (Fig. 2B).

The Kuttara caldera is subcircular (diameter, 3 km) and retains its primary morphological features, such as a caldera rim and inner caldera wall (Fig. 2A). The caldera formed during violent and explosive silicic eruptions at *ca.* 40 ka (Moriizumi, 1998; Yamagata, 1994) that resulted in a large-volume dacitic pyroclastic fall and flow deposits around the caldera (Kt-1 tephra; Yamagata, 1994). Lake Kuttara is 2.5 km in diameter with a maximum depth of 148 m (water level, 258 m above sea level). The lake water is clear and transparent to a depth of 22 m, as measured in 1991 (Environment Agency of Japan, 1993). The caldera has never been drilled, and its subsurface geology is poorly known. Gravity data (Yokoyama *et al*., 1967) show that

*College of Environmental Technology, Graduate School of Engineering, Muroran Institute of Technology, Mizumoto-cho 27−1, Muroran, Hokkaido 050−8585, Japan.
**Neo Science Co. Ltd, Tarui 4−2−30, Sennan, Osaka 590−0521, Japan.

Corresponding author: Yoshihiko Goto
e-mail: ygoto@mmm.muroran-it.ac.jp

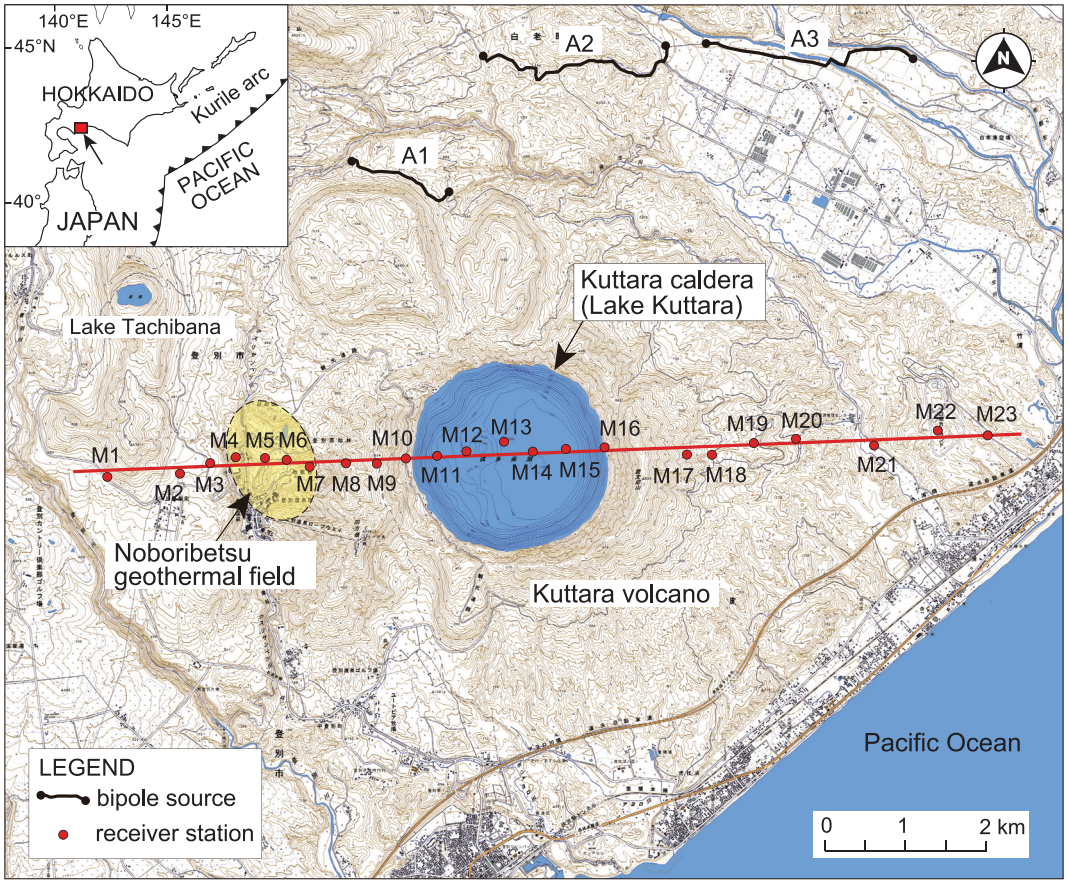

Fig. 1. Location map of the Kuttara volcano, Hokkaido, Japan. The CSAMT survey line (red line) is 12 km long and is oriented E–W, passing over Kuttara caldera (Lake Kuttara) and the Noboribetsu geothermal field. Locations of the bipole sources (A1, A2, and A3; black lines, and black circles showing the locations of electrodes) and receiver stations (red circles; M1−23) are shown. The base map is from the 1:25,000 scale topographic maps (the 'Noboribetsu-onsen' and 'Tobiu' quadrangles), issued by the Geospatial Information Authority of Japan. The topographic contour interval is 10 m.

the caldera has a negative gravity anomaly.

Post-caldera volcanism, which occurred on the western slope of the stratovolcano at *ca.* 15 ka, formed the Noboribetsu geothermal field (Goto and Danhara, 2011; Katsui *et al*., 1988; Fig. 1). The geothermal field (1 × 1.5 km) is characterized by a dacitic cryptodome (the Hiyoriyama cryptodome; 130 m high and 350−550 m across), a number of small explosion craters (up to 210 m across), active fumaroles, and hot springs (Goto *et al*., 2011). Previous geological studies suggest that more than 12 phreatic eruptions have occurred in this field during the past 8500 years (Goto *et al*., 2013).

3. CSAMT survey

The CSAMT survey was conducted to obtain the resistivity structure beneath the Kuttara caldera at depths of up to 1000 m. The survey was conducted along a 12-km-long east–west-trending transect crossing Kuttara volcano and passing over the Kuttara caldera and the Noboribetsu geothermal field (Fig. 1). The CSAMT procedure followed the 'scalar CSAMT' method (Matsuoka, 2005), whereby a transmitter injects electrical currents into the ground at audio and near-audio frequencies via a grounded wire (bipole source), and a receiver records both the electric field parallel to the grounded wire and the magnetic field perpendicular to the wire (Fig. 3A).

The CSAMT survey was conducted using a high-resolution electromagnetic system (Geo-SEM; Neoscience Co. Ltd, Osaka, Japan) consisting of a transmitter and a receiver (Fig. 4A and B). The transmitter (Fig. 4A) consisted of a transformer, rectifier, switching circuit, GPS clock, and generator. The grounded wire connected to the transmitter was 1.3−2.6 km long and contained 30 electrodes at each termination (each electrode consisted of a stainless steel rod, 600 mm long and 13 mm across) (Fig. 3A). The receiver (Fig. 4B) comprised an amplifier, filter, data

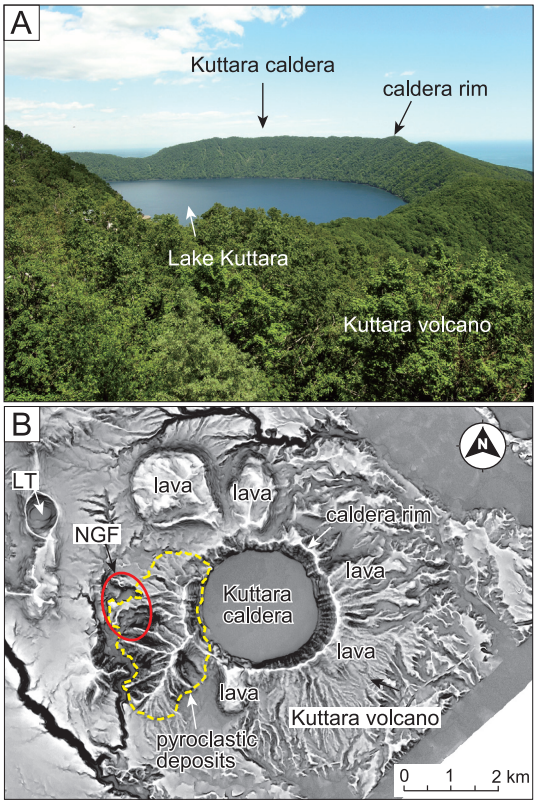

Fig. 2. (A) Photograph of the Kuttara caldera viewed from the southwest. The caldera contains a circular freshwater lake (Lake Kuttara), 2.5 km across. (B) Three-dimensional topographic image of Kuttara volcano showing its main geological features. The northern, eastern, and southern parts of the volcano are comprised mainly of andesitic lavas, whereas the western part is comprised of dacitic pyroclastic deposits (within the broken yellow line). The Noboribetsu geothermal field (NGF) lies on the western slope of the volcano (red circle). LT, Lake Tachibana (volcanic crater). The base map is from the red relief image map, RRIM10 of Asia Air Survey (Chiba *et al*., 2007), using 10-m DEM data of the Geospatial Information Authority of Japan (GSI).

logger, GPS clock, and set of sensors. The sensors consisted of a pair of electrodes and a coil; each electrode consisted of a copper rod, 280 mm long and 15 mm across. The transmitter and receiver were synchronized using a high-precision GPS quartz clock system to an accuracy of 1×10^{-6} s. The specifications of the Geo-SEM system are given in Table 1; further details of the system are described in Johmori *et al*., (2010).

The CSAMT survey line was 12 km long and oriented N88° E. The 23 receiver stations (M1−23) were horizontally spaced at intervals of 300−1000 m (Fig. 1); M1−9

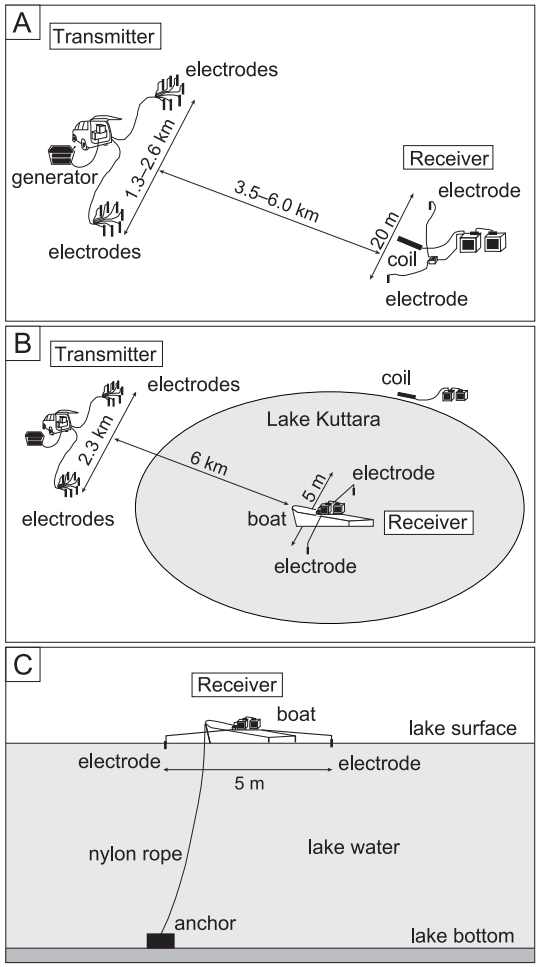

Fig. 3. (A) Schematic diagram of the electromagnetic system (Geo-SEM) used for the CSAMT survey for on-land stations (stations M1−10 and M16−23). The bipole sources (grounded wire) for the transmitters are 1.3−2.6 km long and have 30 electrodes at each termination. The receiver has a set of sensors consisting of a pair of electrodes and a coil. The distances between the grounded wire and receiver stations were 3.5−6.0 km. (B) Schematic diagram of the CSAMT resistivity survey on Lake Kuttara (stations M11−15), obtained by on-boat measurements. A pair of electrodes (distance, 5 m) was set at either end of surveying poles that extended from the boat, which were adjusted parallel to the bipole source to measure the electric field. The coil was set at the nearest lakeshore. (C) Cross-section of the CSAMT resistivity survey on Lake Kuttara. The boat is fixed to the measuring location with an anchor.

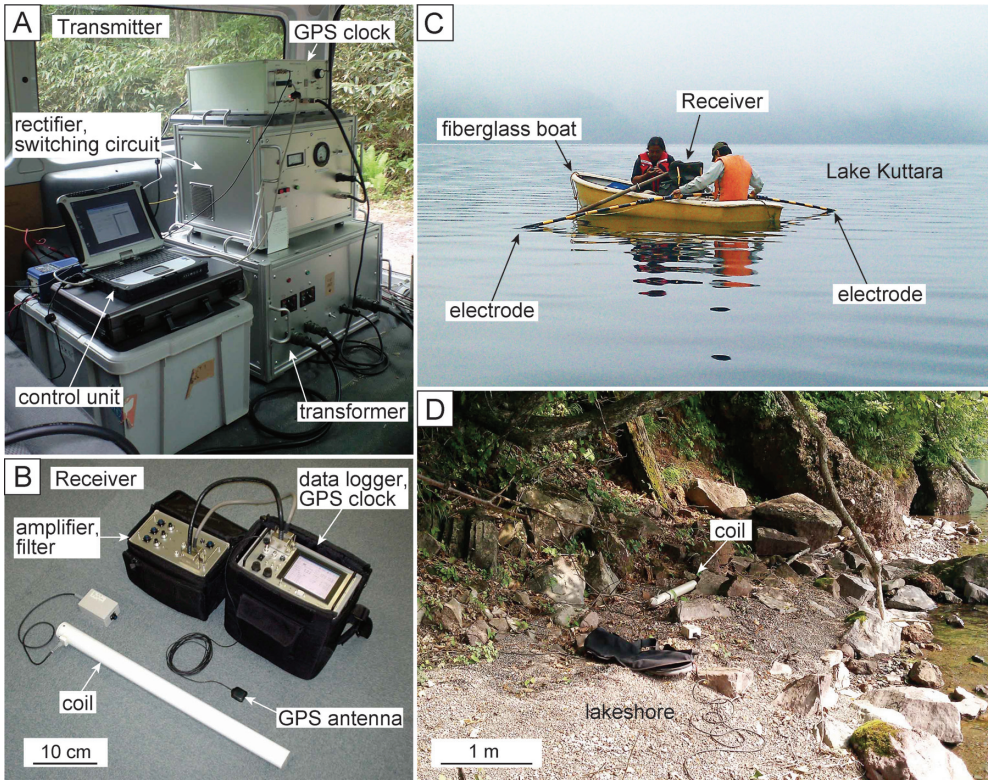

Fig. 4. (A) Photograph of the transmitter of the electromagnetic system (Geo-SEM) used for the CSAMT survey. (B) A Geo-SEM receiver. The white coil is 72 cm long. (C) CSAMT survey on Lake Kuttara (receiver station M11; Fig. 1). A manned fiberglass boat was used to measure the electric field on the lake. A pair of electrodes (distance, 5 m) was set at either end of surveying poles that extended from the boat. (D) A coil was set on the lakeshore to measure the magnetic field (M16 station, for substituting the magnetic fields at M13, M14 and M15).

Table 1. Specifications of the exploration system used for the CSAMT survey (Geo SEM).

CSAMT survey system (Geo SEM)	
Transmitter	
Output power	5 kW (maximum)
Output voltage	1000 V (maximum)
Output current	10 A (maximum)
Frequency	1, 2, 4, 8, 16, 32, 64, 128, 256, 512, 1024, 2048, 4096, 8192 Hz
	20, 40, 80, 160, 320, 640, 1280, 2560, 5120 Hz
Generator	6 kW (maximum), 200V AC, 60 Hz, 3 phase
Receiver	
Frequency	1, 2, 4, 8, 16, 32, 64, 128, 256, 512, 1024, 2048, 4096, 8192 Hz
	20, 40, 80, 160, 320, 640, 1280, 2560, 5120 Hz
Channel	3 or 5 channels
Amplification degree	0–90 dB (10 dB pitch)
Wave analysis	stacking, Fourier transform

were located on the western slope of the stratovolcano (M4−7 being located in the Noboribetsu geothermal field), M10−16 were located in the Kuttara caldera (M11−15 being located on Lake Kuttara), and M17−23 were located on the eastern slope of the stratovolcano. Positions of the receiver stations were determined by GPS.

The bipole sources (grounded wires) were placed at three locations (A1, A2, and A3; Fig. 1) so as to cover the entire 12-km length of the survey line. Source A1 (for measurements at M1−10) was 1.3 km long and oriented N73° W. Source A2 (for measurements at M11−16) was 2.3 km long and oriented N87° E. Source A3 (for meas-

urements at M17−23) was 2.6 km long and oriented N86° W. The distances between the bipole sources and the receiver stations were as follows: 3.5−6.0 km between A1 and M1−10, 6.0 km between A2 and M11−16, and 6.0 km between A3 and M17−23.

The resistivity measurements were carried out in two different ways, depending on whether the receiver station was on land or water. At stations on land (M1−10 and M16−23), the electrodes and coil were placed on the ground surface (Fig. 3A). A pair of electrodes (separated by a distance of 20 m) were set parallel to the bipole source to measure the electric field, whereas the coil was set perpendicular to the bipole source to measure the magnetic field. At stations on Lake Kuttara (M11−15), a manned fiberglass boat (4.5 m long, 1.5 m wide) was floated on the lake (Figs. 3B and 4C) and anchored at each measuring location (Fig. 3C). A pair of electrodes (each consisting of a copper rod, 280 mm long and 15 mm across) was mounted at either end of a surveying pole that extended from the boat (separation distance, 5 m). The poles were adjusted so that they were parallel to the bipole source, so that the electrodes could correctly measure the electric field (Fig. 4C). The on-boat measurements of the electric field were possible because the waves on the lake were sufficiently small that their effect on the electric field measurements was minor. In contrast, measurements of the magnetic field were significantly influenced by small waves, and therefore for magnetic measurements the coil was placed on the ground surface on the lake shore (locations M10 and M16; Fig. 1), and was set perpendicular to the bipole source (Fig. 4D). We substituted the magnetic field at M10 for the fields at M11 and 12, and substituted the magnetic field at M16 for the fields at M13, 14, and 15. These substitutions were based on the observation that magnetic fields up to a given distance from a bipole source were nearly identical, assuming the resistivity structure to be 1-D or 2-D. Suzuki *et al.* (2009) performed a similar on-lake CSAMT survey on a dammed lake. The on-boat survey method is environmentally friendly and inexpensive.

The CSAMT survey was conducted between 20 July and 2 August 2011. The transmitter injected 1−8-A electrical currents into the ground at frequencies of 1, 2, 4, 8, 16, 32, 64, 128, 256, 512, 1024, 2048, 4096, and 8192 Hz, and another series at frequencies of 20, 40, 80, 160, 320, 640, 1280, 2560, and 5120 Hz, to minimize noise related to the commercially used frequency of 50 Hz and its associated higher harmonics. The receiver recorded the electric and magnetic fields parallel and perpendicular to the grounded wire, respectively. The measurement time at each receiver station was 1 hour (minimum of 2 minutes at 8192 Hz; maximum of 8 minutes at 1 Hz).

The CSAMT data were processed using a band-pass filter, a Fourier transform, and stacking to remove noise. The number of waves for stacking was $>$400,000 at 8192 Hz to $>$300 at 1 Hz. The apparent resistivity and phase were then calculated from the electric and magnetic fields. Measurement errors for the apparent resistivity and phase were not calculated because to increase the resolution frequency, the frequency analyses of the CSAMT data were performed for long time-series of data that had not been divided into plural datasets (see Johmori *et al*., 2010).

The quality of the data at each measurement station was checked by examining the ρ_a–f curve, where ρ_a is the apparent resistivity and f is the frequency. The ρ_a–f curves for stations M1 and M3−23 were smooth, and generally exhibited an increase in apparent resistivity in direct proportion to the frequency. The smooth curves imply that the data from stations M1 and M3−23 are acceptable for resistivity calculations. In contrast, the ρ_a–f curve for M2 showed an abrupt decline in apparent resistivity at around 50 Hz, which is the commercial frequency in this area, implying that the M2 data were influenced by artificial noise. The M2 station is located near a high-voltage power line; therefore, the M2 data were rejected.

The possibility of discrepancies in the data caused by the use of three bipole sources with slightly different azimuths (A1, N73° W; A2, N87° E; A3, N86° W) was also considered. Two sets of data, measured at station M10 station using sources A1 and A2, were compared using the ρ_a–f and ϕ–f curves, where ϕ is the phase angle and f is the frequency. The curves were in good agreement with one another, indicating that discrepancies related to source azimuth angles were absent or minimal.

Given the short distances between the bipole source and the receivers for stations M3−10 (3.5−4.5 km), the low-frequency data ($<$8 Hz) at these stations could potentially be affected by the near-field effect (*cf.* Sandberg and Hohmann, 1982). Therefore, after checking the CSAMT data, a near-field correction was applied to the CSAMT data, following the method of Sasaki (1988). The corrected CSAMT data (apparent resistivity and phase angles) are shown in Fig. 5.

4. Data analysis

The resistivity structure beneath the Kuttara volcano was calculated using a 2-D inversion of the CSAMT data, assuming a 2-D structural model. The 2-D inversion was performed using a finite element method (following Sasaki, 1986) by setting the results of the 1-D inversion as the initial model. The 1-D-inversion model was determined from the apparent resistivity and phase angles of the CSAMT data, using a non-linear least-square method based on the analytical theory of Ward and Hormann (1987).

The 2-D inversion was performed in transverse magnetic (TM) mode (Sasaki, 1986) along a 12-km-long section oriented N88° E (survey line, Fig. 1). The amount of calculation required for the 2-D inversion of this section was beyond the capacity of our computing resources. We

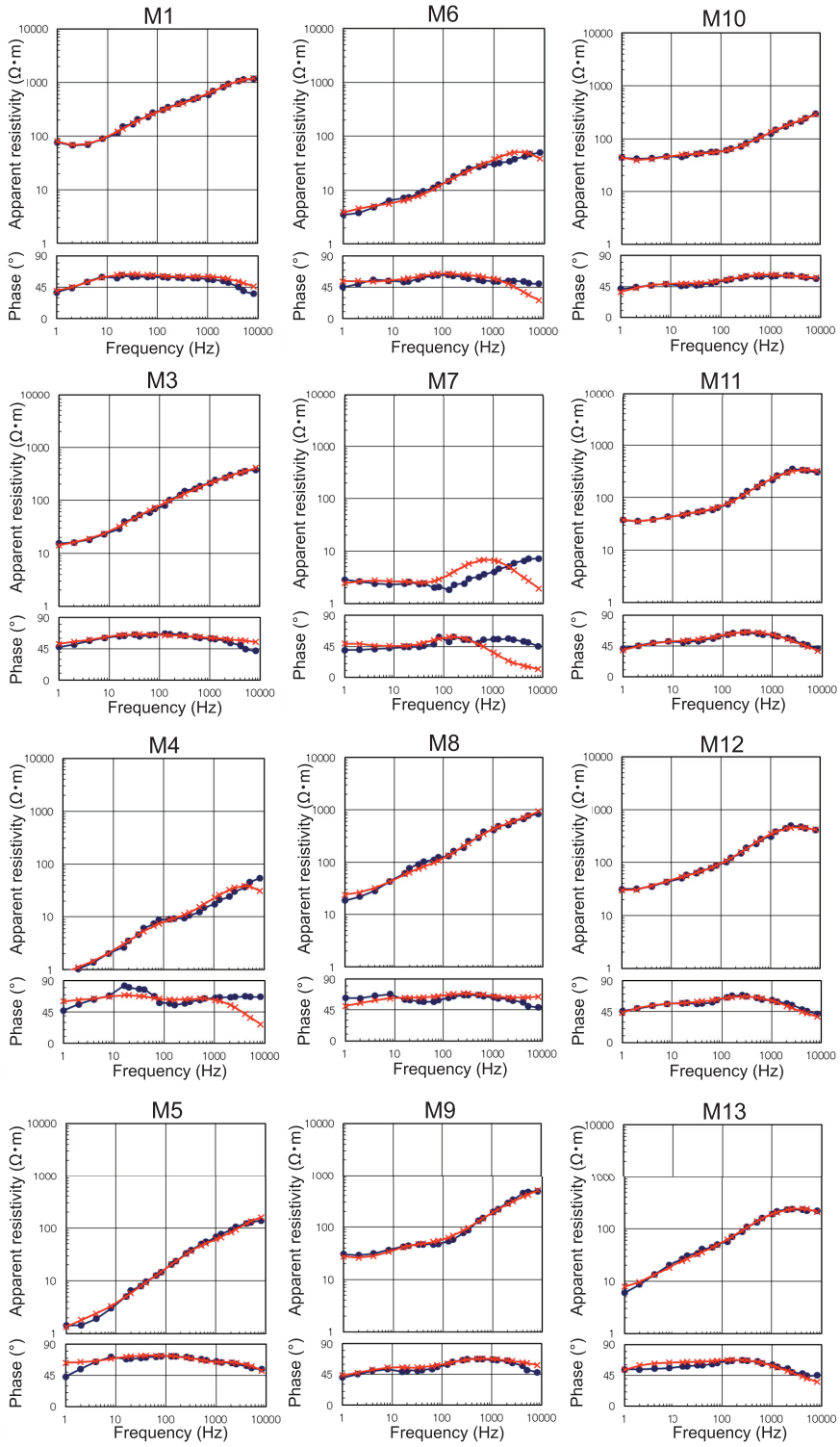

Fig. 5. Apparent resistivity and phase angles of the obtained CSAMT responses (blue lines) and the calculated responses for the apparent resistivity and phase angles (red lines) for receiver stations M1−23 (see Fig. 1 for station location). The M2 data are not shown because of the influence of artifacts due to 50-Hz commercial noise (see Section 3).

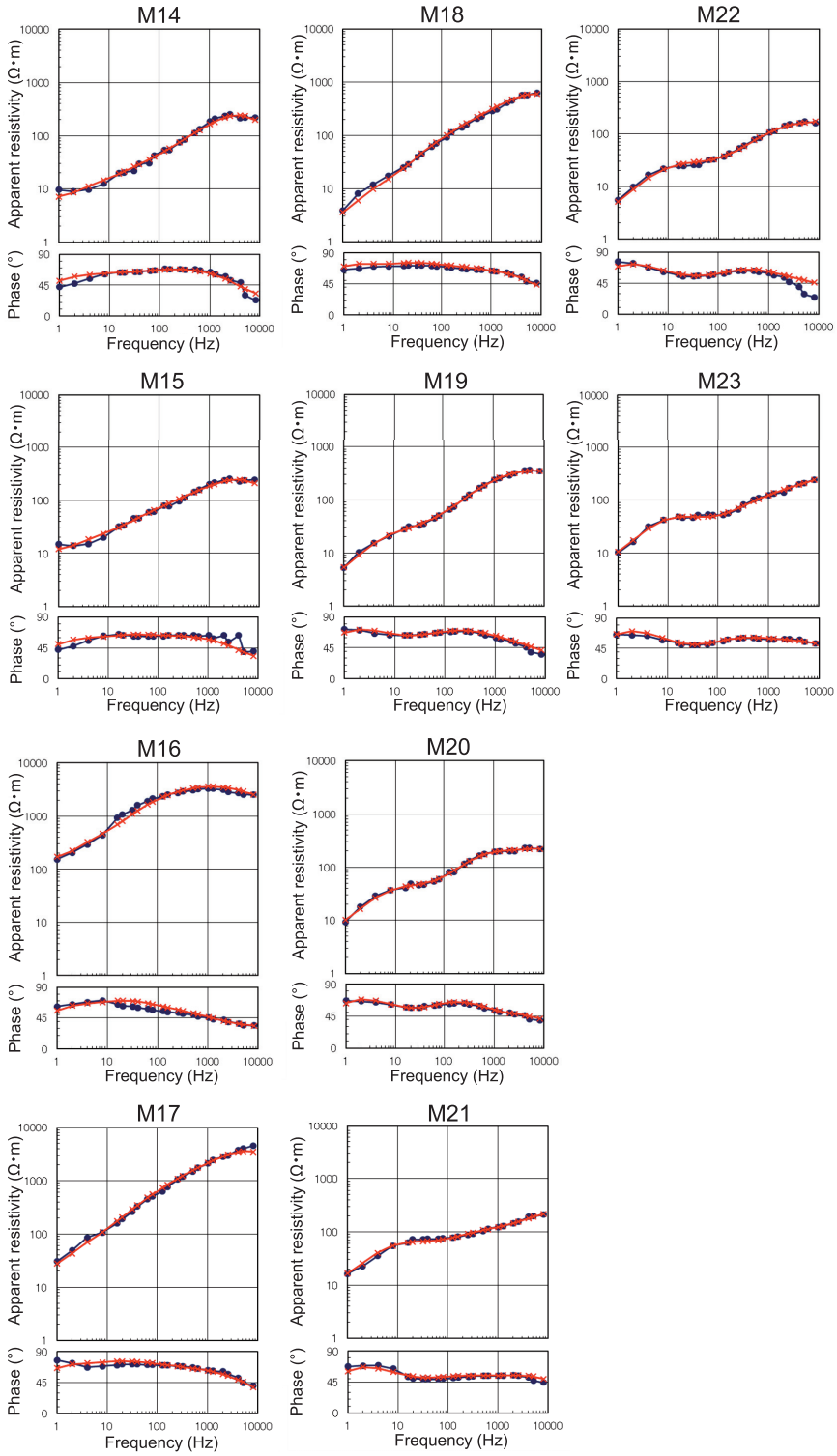

Fig. 5. Continued.

therefore divided the section into three parts (M1−12, M9−18, and M17−23) and performed the calculations for each part separately. The 2-D inversion results for the three parts were then joined together (at 4000 m and 8300 m from the western termination of the survey line) to reform the 12-km-long section. No discrepancies were observed between the calculated results (resistivity models) at the positions of the joined segments.

The 2-D inversion included a topographic model constructed from elevation data of 1:25,000 scale topographic maps (the 'Noboribetsu-onsen' and 'Tobiu' quadrangles) issued by the Geospatial Information Authority of Japan. The mesh size of the finite element method was 20 m (element size, 20 × 20 m). Each 'inversion block', which represents the unit used in the 2-D inversion to calculate resistivity (Sasaki, 1986), consisted of four elements. The 2-D inversion was performed by comparing the field data (apparent resistivity and phase angles) with the calculated results, using a non-linear least-squares method. The iteration for the 2-D inversion was run eight times. The 2-D inversion reduced the effects of topography on the CSAMT data. The 2-D inversion may also have reduced distortions of the resistivity structure due to static shifts.

Figure 5 shows that the obtained CSAMT responses (apparent resistivity and phase angles) were in overall agreement with the calculated responses, except for values of the response at station M7, located on the edge of the Noboribetsu geothermal field, which showed differing values at high frequencies. These differences were probably the result of the steep rugged topography at this station; however, the station is located far from the Kuttara caldera, and thus the differences should not have adversely impacted the results of the resistivity structure beneath the caldera.

A root mean square (RMS) value was calculated from the obtained CSAMT responses (apparent resistivity) and the calculated responses to quantitatively investigate the match between them. Phase values were not used in the calculations, as the phase is functionally dependent on the apparent resistivity. The RMS value (δ) is defined as $\delta = [\sum \{\ln(\rho_a f) - \ln(\rho_a c)\}^2/n]^{1/2}$, where $\rho_a f$ is the obtained CSAMT response (apparent resistivity), $\rho_a c$ is the calculated response, and n is the number of measurements. According to this definition, an RMS value of zero indicates that the calculated response perfectly matches the obtained CSAMT response, whereas an RMS value of 0.1 indicates that ~90 % of the calculated response matches the obtained CSAMT response (i.e., ~10 % error). The RMS values were calculated for three data sets (M1−12, M9−18, and M17−23). The obtained RMS values are 0.133 for M1−12, 0.084 for M9−18, and 0.046 for M17−23, indicating a good agreement between the obtained CSAMT responses and the calculated responses.

Depth of penetration was determined from the skin depth (Cagniard, 1953) and the Bostick depth (Murakami, 1987). The skin depth is defined as the depth at which the amplitude of electromagnetic waves decreases to 1/e, where e is the base of the natural logarithm. The Bostick depth is defined as $1/\sqrt{2}$ of the skin depth, and is considered to represent a more accurate depth of penetration than the skin depth. The skin depth calculated from the frequency of electric currents for the deepest layer (1 Hz), and from the corresponding apparent resistivity (mostly 10−100 Ω·m) for the CSAMT data, yields depths of penetration of 1500−5030 m, while the Bostick depth calculated from the same data yields penetration depths of 1060−3556 m. The depth of penetration was therefore conservatively considered to be 1000−1500 m below the ground surface.

5. Results

Processing of the CSAMT data revealed the subsurface resistivity structure beneath Kuttara volcano, including Kuttara caldera, to depths of up to 1000 m below the surface (Fig. 6A). Prominent features of the resistivity structure (outlined in Fig. 6B) are: a layer of high resistivity extending along or near the ground surface across the entire volcano (zone A); a layer of high resistivity at Lake Kuttara (zone B); a columnar region of low resistivity beneath Lake Kuttara (zone C); a broad columnar region of low resistivity beneath the Noboribetsu geothermal field (zone D); and an extensive region of low resistivity at depth below the eastern part of the volcano (zone E).

Among these zones, zone C is of particular importance for understanding the caldera's internal structure because it is located just beneath the caldera. We therefore performed a sensitivity test for zone C, by substituting a virtual resistivity value of 20 Ω·m for the original resistivity value, and re-calculating the RMS value for M9−18 (the value of 20 Ω·m was based on the resistivity value around zone C). The sensitivity test resulted in an increase in the RMS value to 0.142, as compared with the original RMS value of 0.084, indicating the reliability of our results regarding the existence of zone C.

6. Geological interpretations

Generally, the resistivity of rocks and sediments is lowered by the presence of conductive minerals (*e.g.*, alteration minerals such as smectite-series clays), thermal waters in pores and fractures, and high temperatures (*e.g.*, Milsom, 2003; Takakura, 1998). These observations, suggesting that resistivity data show marked changes in the vicinity of hydrothermal alteration zones and faults (*e.g.*, Martyn *et al*., 1997; Risk *et al*., 2003), are the basis for the geological interpretations of the five zones (A–E in Fig. 6B) presented below. Because the resistivity section obtained in this study (Fig. 6A) offers only a two-dimensional perspective, we have combined the data with the distribution of topographic features to make inferences regarding the architecture of the caldera, particularly with

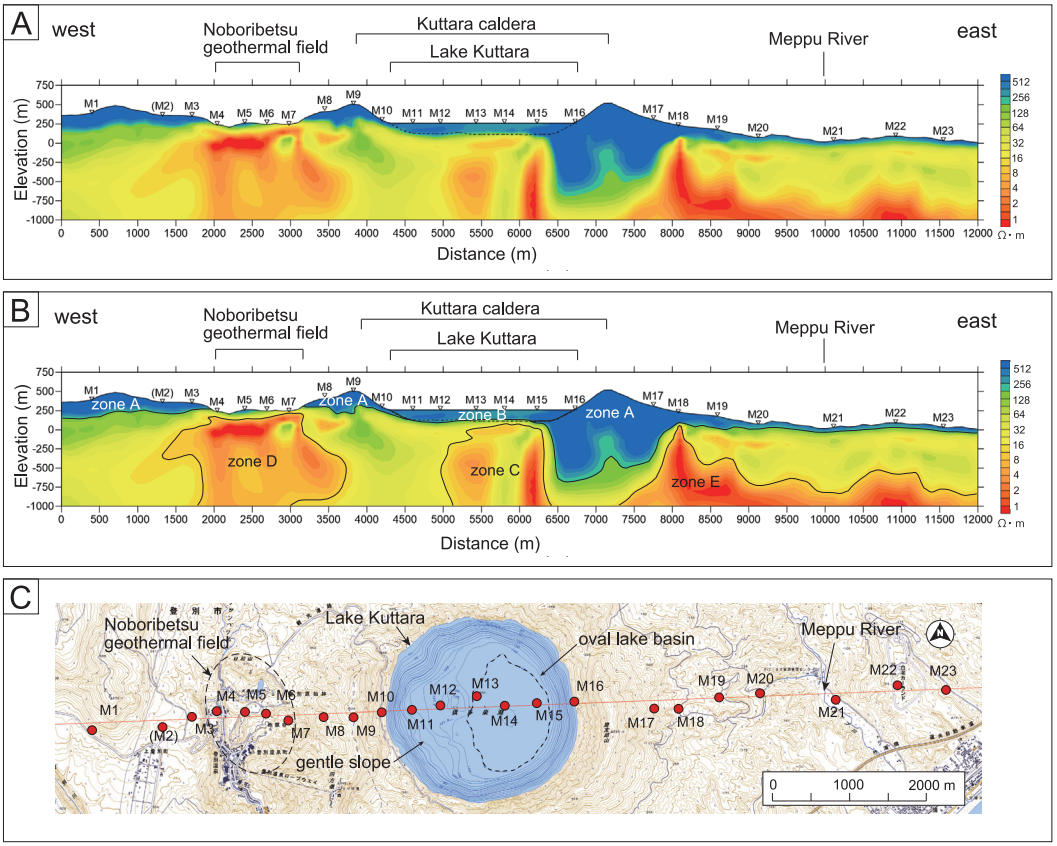

Fig. 6. (A) Resistivity structure beneath the Kuttara volcano, including the Kuttara caldera, calculated by a 2-D inversion. (B) Annotated version of the resistivity structure, showing zones A–E. Zone A is interpreted to represent andesitic lavas, scoria, and pyroclastic deposits. Zone B corresponds to lake water. Zone C is inferred to be a domain filled with lava blocks and pyroclasts, which subsided during caldera collapse and were subject to hydrothermal alteration. Zone D is interpreted to be a hydrothermally altered zone beneath the Noboribetsu geothermal field. Zone E is inferred to be a hydrothermally altered zone. (C) Topographic map showing locations of the receiver stations and the main bathymetric features at the bottom of Lake Kuttara.

respect to the three-dimensional extent of geological structures.

Zone A (resistivity＞100 Ω·m) extends subhorizontally along the ground surface and varies in thickness from 200 m at the western part of Kuttara volcano to 800 m at the eastern part. The surface of the volcano consists of fresh andesitic lavas, andesitic scoria, and minor dacitic pyroclastic deposits (Katsui *et al.*, 1988; Moriizumi, 1998), suggesting that zone A corresponds to these rock types. The andesitic lavas and scoria are distributed mainly in the northern, eastern, and southern parts of the volcano, whereas the dacitic pyroclastic deposits are distributed in the western part (Fig. 2B; Katsui *et al.*, 1988; Moriizumi, 1998). Variations in the thickness of zone A may reflect these changes in rock type.

Zone B (resistivity＞100 Ω·m), which is 2500 m wide and ~150 m thick, coincides with the location of Lake Kuttara, which is 2.5 km across and 130−148 m deep. This suggests that zone B corresponds to lake water, as the high resistivity values (＞100 Ω·m) are consistent with those of fresh (non-salt) water. The resistivity of lake water sampled from the lake surface in July 2011 and measured in our laboratory was 143.5 Ω·m, which is consistent with the interpretations of the field data. The correspondence between the lake depth (130−148 m) and the thickness of zone B (~150 m) indicates that the results of the on-board CSAMT survey on Lake Kuttara are reliable.

Zone C (resistivity＜30 Ω·m) is located beneath Kuttara caldera, and extends subvertically for up to 1000 m and is 1300−1500 m wide. Because of its location beneath the caldera, we interpret this zone as a domain filled with lava blocks and pyroclasts that subsided during caldera collapse and was subjected to hydrothermal alteration. Zone C comprises a higher-resistivity core (10−30 Ω·m) and a

lower-resistivity rim (< 10 Ω·m), a structure that could reflect the stability and presence of smectite (stable at temperatures of <200℃; Aizawa *et al*., 2008, 2009; Lee *et al*., 2010; Takakura *et al*., 2000), showing that smectite is absent in the core of the domain but present on its edges. The eastern boundary of zone C is sharp and linear, suggesting the presence of a distinct subvertical fault (probably a ring fault) at the eastern edge of the domain. The western boundary of zone C is diffuse, suggesting a gradual geological contact or the presence of an indistinct ring fault.

Zone C is located toward the eastern edge of Lake Kuttara rather than at the center of the lake. Bathymetric isobaths (Fig. 6C) indicate that an oval basin is present in the eastern part of the lake (1000×1500 m, elongate N–S) and that this basin represents the deepest part of the caldera; the western part of the caldera, on the other hand, is tilted gently to the east and has a relatively irregular surface. The location of zone C thus corresponds to the location of the oval basin, suggesting that this was the center of caldera collapse. This inference is consistent with the gravity data of Yokoyama *et al.* (1967), who reported a negative gravity anomaly (1.5 milligal low) at the eastern center of the caldera floor, indicating the existence of low-density materials at depth. Topographic data (Fig. 2B) show that a steep curviplanar cliff demarcates the eastern inner caldera wall, whereas the western caldera wall is slightly irregular and has several scallop-shaped indents. We thus infer that the western caldera rim was significantly enlarged as a result of landsliding during caldera formation.

Zone D (resistivity < 5 Ω·m) is located beneath the Noboribetsu geothermal field, and extends subvertically for up to 1000 m and is 1000−1500 m wide. Because of its location beneath the geothermal field, we interpret that zone D is a hydrothermal alteration zone produced by upwelling high-temperature fluids (Goto and Johmori, 2011). The location and size of the hydrothermal alteration zone are consistent with the distribution of geothermal features observed at the surface of the geothermal field (*e.g.*, active fumaroles, hot springs, and hydrothermal alteration zones). Notably, zones C and D are distinct and separate entities beneath the Kuttara caldera and the Noboribetsu geothermal field, respectively (Fig. 6B). The distance between them (1500−2000 m) implies that, at least within the vertical resolution of the data (up to 1000 m below the surface), different pathways exist for the ascent of high-temperature fluids beneath Kuttara volcano.

Zone E (resistivity < 5 Ω·m) is located beneath the eastern slope of Kuttara volcano and extends subhorizontally for more than 4000 m at a depth of ~1000 m. We cannot provide an adequate interpretation for this low-resistivity region, as no drilling data are available from this area (NEDO, 1991); however, the occurrence of hydrothermal alteration may provide a possible explanation for the zone. Zone E extends sharply upward below station M18 (Fig. 6B), a feature which could represent the existence of a fault. Zones D and E are both roughly symmetrical with respect to the Kuttara caldera, suggesting that they may represent hydrothermal alteration developed along large concentric fractures (~5.5 km across) encircling the Kuttara caldera.

7. Discussion

The resistivity structure obtained in this study (Fig. 6B) reveals that the internal structure of the Kuttara caldera is asymmetric. We infer that caldera collapse occurred below the eastern part of the caldera floor and that the perfect circular outline of Lake Kuttara resulted from the enlargement of the western caldera rim due to mass wasting processes during caldera formation. Such asymmetric structures are common in relatively small calderas, such as in Miyakejima, Japan (Geshi, 2009). Asymmetric structures have also been reported in ancient eroded calderas (*e.g.*, Kumano, Japan; Miura, 1999). Analog modeling experiments simulating caldera collapse (*e.g.*, Geyer *et al*., 2006; Kennedy *et al*., 2004) also suggest that caldera subsidence commonly begins with a downsag flexure (Branney, 1995) followed by the formation of an asymmetric ring fault. We infer that the asymmetric internal structure of the Kuttara caldera is caused by geological heterogeneities within the volcano, whereby the eastern part comprises mainly andesitic lavas and the western part comprises mainly dacitic pyroclastic deposits. As suggested earlier, the thickness variation of zone A (Fig. 6B) may reflect these variations in rock type.

Asymmetric caldera collapse was well documented during the 2000 AD eruption of Miyakejima volcano, Japan (Geshi, 2009; Geshi *et al*., 2002). There, a small circular caldera (1.6 km across) was formed by asymmetric subsidence of the volcano summit and by repeated landsliding, rockfall, and small-scale debris avalanching of the resultant caldera wall. Caldera subsidence occurred mainly in the northwestern part of the caldera floor, whereas the mass wasting processes occurred mainly in the southeastern part of the caldera. The resulting caldera was asymmetric, contained an oval basin in the northwestern part of the caldera floor (600×800 m, elongate NE–SW), and had a steep slope in its southeastern part. Geshi (2009) suggested that asymmetric collapse at the Miyakejima 2000 caldera was a result of the heterogeneous structure of the volcano. The Kuttara caldera shares similarities to the Miyakejima 2000 caldera in terms of its size and morphology; thus, based on this modern-day analogue we suggest the Kuttara caldera was produced by similar asymmetric subsidence and mass-wasting processes.

8. Conclusions

A CSAMT survey revealed the subsurface resistivity structure of the caldera on Kuttara volcano at depths of up

to 1000 m. The resistivity structure showed that the internal structure of the caldera is asymmetric. Caldera collapse occurred beneath an oval basin located toward the eastern part of the caldera floor, and the western caldera rim was significantly enlarged as a result of landsliding during caldera formation. The asymmetry of caldera collapse may be attributed to geological heterogeneities within the volcano.

Acknowledgements

This research was sponsored by the Ministry of Education, Culture, Sports, Science and Technology of Japan (MEXT), and was supported financially by the Muroran Institute of Technology. We thank N. Johmori, T. Kondou, and T. Takahashi (Neoscience Co. Ltd) for assistance in the field, and K. Kizaki (Docon Co. Ltd) for constructive discussions on the geology of Kuttara caldera. Comments by N. Geshi (AIST), an anonymous referee, and editing by K. Aizawa (Kyushu University) significantly improved the manuscript.

References

Aizawa, K., Ogawa, Y., Hashimoto, T., Koyama, T., Kanda, W., Yamaya, Y., Mishina, M. and Kagiyama, T. (2008) Shallow resistivity structure of Asama volcano and its implications for magma ascent process in the 2004 eruption. *J. Volcanol. Geotherm. Res*., **173**, 165−177.

Aizawa, K., Ogawa, Y. and Ishido, T. (2009) Groundwater flow and hydrothermal systems within volcanic edifices: Delineation by electric self-potential and magnetotellurics. *J. Geophys. Res*., **114**, doi: B0120810.1029/2008jb005910.

Branney, M.J. (1995) Downsag and extension at calderas: new perspectives on collapse geometries from ice-melt, mining, and volcanic subsidence. *Bull. Volcanol*., **57**, 303−318.

Cagniard, L. (1953) Basic theory of the magneto-telluric method of geophysical prospecting. *Geophysics*, **18**, 605−635.

Chiba, T., Suzuki, Y. and Hiramatsu, T. (2007) Digital terrain representation methods and red relief map, a new visualization approach. *J. Japan Cartographic Association (Map)*, **45**, 27−36. (in Japanese with English abstract)

Environment Agency of Japan (1993) **The 4th environmental investigations on lakes and swamps of Japan**. Nature Conservation Bureau of the Environment Agency, Tokyo, 188p. (in Japanese)

Geshi, N. (2009) Asymmetric growth of collapsed caldera by oblique subsidence during the 2000 eruption of Miyakejima, Japan. *Earth Planet. Sci. Lett*., **280**, 149−158.

Geshi, N., Shimano, T., Chiba, T. and Nakada, S. (2002) Caldera collapse during the 2000 eruption of Miyakejima Volcano, Japan. *Bull. Volcanol*., **64**, 55−68.

Geyer, A., Folch, A. and Marti, J. (2006) Relationship between caldera collapse and magma chamber withdrawal: an experimental approach. *J. Volcanol. Geotherm. Res*., **157**, 375−386.

Goto, Y. and Danhara, T. (2011) Zircon fission-track dating of the Hiyoriyama Cryptodome at Kuttara Volcano, southwestern Hokkaido, Japan. *Bull. Volcanol. Soc. Japan*, **56**, 19−23.

Goto, Y. and Johmori, A. (2011) Controlled source audio-frequency magnetotelluric (CSAMT) and time domain electromagnetic (TDEM) resistivity measurements at Noboribetsu Geothermal Field, Kuttara Volcano, Hokkaido, Japan. *Bull. Volcanol. Soc. Japan*, **56**, 153−160.

Goto, Y., Matsuzuka, S. and Kameyama, S. (2011) Three-dimensional digital mapping of Noboribetsu Geothermal Field, Kuttara Volcano, Hokkaido, Japan, using helicopter-borne high-resolution laser scanner. *Bull. Volcanol. Soc. Japan*, **56**, 127−135.

Goto, Y., Sasaki, H., Toriguchi, Y. and Hatakeyama, A. (2013) History of phreatic eruptions in the Noboribetsu Geothermal Field, Kuttara Volcano, Hokkaido, Japan. *Bull. Volcanol. Soc. Japan*, **58**, 461−472.

Johmori, A., Mitsuhata, Y., Nishimura, S., Johmori, N., Kondou, T. and Takahashi, T. (2010) Development of a deep electromagnetic exploration instrument with high frequency spectrum resolution using GPS synchronization. *J. Japan Soc. Engin. Geol*., **51**, 62−72. (in Japanese with English abstract)

Katsui, Y., Yokoyama, I., Okada, H., Abiko, T. and Muto, H. (1988) **Kuttara (Hiyoriyama), its volcanic geology, history of eruption, present state of activity and prevention of disasters**. Committee for Prevention and Disasters of Hokkaido, Sapporo, 99 p. (in Japanese)

Kennedy, B., Styx, J., Vallance, J. W., Lavallee, Y. and Longopre, M. A. (2004) Controls on caldera structure: results from analog sandbox modeling. *GSA Bulletin*, **106**, 515−524.

Lee, J.O., Kang, I.M. and Cho, W.J. (2010) Smectite alteration and its influence of the barrier properties of smectite clay for a repository. *Applied Clay Science*, **47**, 99−104.

Martyn, J., Unsworth, M.J., Malin, P.E., Egbert, G.D. and Booker, J.R. (1997) Internal structure of the San Andreas fault at Parkfield, California. *Geology*, **25**, 359−362.

Matsuoka, T. (2005) **Dictionary of exploration geophysics.** Society of Exploration Geophysics of Japan ed., Aichi Shuppan, Tokyo, 279p. (in Japanese)

Milsom, J. (2003) **Field Geophysics**. John Wiley and Sons, England, 232p.

Miura, D. (1999) Arcuate pyroclastic conduits, ring faults and coherent floor at Kumano caldera, southwest Honshu, Japan. *J. Volcanol. Geotherm. Res*., **92**, 271−294.

Moriizumi, M. (1998) The growth history of the Kuttara volcanic group. *Bull. Volcanol. Soc. Japan*, **43**, 95−111. (in Japanese with English abstract)

Moriya, I. (2003) Kuttara Volcano. In *Regional Geomorphology of the Japanese Islands, vol. 2, Geomorphology of Hokkaido* (Koaze T., Nogami, M., Ono, Y. and Hirakawa. K. eds.), 279−281, University of Tokyo Press, Tokyo. (in Japanese)

Murakami, Y. (1987) Bostic inversion. *Butsuri-Tansa*, **40**, No. 4, 282−291. (in Japanese)

NEDO (New Energy and Industrial Technology Development

Organization) (1991) **Noboribetsu, Report of promotional exploration for geothermal research**, No. 22. NEDO, Tokyo, 845p. (in Japanese)

Risk, G.F., Caldwell, T.G. and Bibby, H.M. (2003) Tensor time domain electromagnetic resistivity measurements at Ngatamariki geothermal field, New Zealand. *J. Volcanol. Geotherm. Res*., **127**, 33–54.

Sandberg, S.K. and Hohmann, G.W. (1982) Controlled-source audiomagnetotellurics in geothermal exploration. *Geophysics*, **47**, 100–116.

Sasaki, Y. (1986) Resolving power of MT method for two-dimensional structures. *Butsuri-Tansa*, **39**, No. 4, 1–9. (in Japanese with English abstract)

Sasaki, Y. (1988) Interpretation of CSAMT data including source effect. *Butsuri-Tansa*, **41**, No. 1, 27–34. (in Japanese with English abstract)

Suzuki, K., Oyama, T., Kawashima, F., Tsukada, T. and Jyomori, A. (2009) Monitoring of grout material injected in bedrock using electrical and electromagnetic exploration. *Proceedings of the 9th SEGJ International Symposium –Imaging and Interpretation–, Sapporo, Japan. 12–14 October 2009*. CD-ROM.

Takakura, S. (1998) Resistivity. In *Handbook for geophysical exploration* (Society of Exploration Geophysics of Japan ed.), 244–247, Society of Exploration Geophysics of Japan. (in Japanese)

Takakura, S., Kozake, K., Nishizawa, O. and Aoki, M. (2000) Resistivity measurement of clay-bearing samples. *Butsuri-Tansa*, **53**, No. 2, 119–128. (in Japanese with English abstract)

Ward, S. H. and Hohmann, G. W. (1987) Electromagnetic theory for geophysical application. In: *Electromagnetic methods in applied geophysics* (Nabighian, M. ed), 131–311, Society of Exploration Geophysics (SEG), Oklahoma.

Yamagata, K. (1994) Tephrochronological study on the Shikotsu and Kuttara Volcanoes in southwestern Hokkaido, Japan. *J. Geogr.*, **103**, 268–285. (in Japanese with English abstract)

Yokoyama, I., Nakai, S., Nishida, Y. and Hirota, T. (1967) Gravity anomaly on Kuttara Caldera Lake in Hokkaido. *Geophys. Bull. Hokkaido Univ.*, **17**, 23–31. (in Japanese with English abstract)

(Editional handling Koki Aizawa)

北海道南西部クッタラカルデラの内部構造

後藤芳彦・城森　明

北海道南西部に位置するクッタラカルデラは，クッタラ火山の山頂部に形成された径約 3 km の小型カルデラである．このカルデラの内部構造を解明するため，CSAMT 法による比抵抗構造探査を行った．探査はクッタラカルデラを東西方向に横断する測線上（測線長 12 km，受信点 23 箇所）で行い，カルデラ内のクッタラ湖では小型ボートを用いた湖上測定を行った．データ解析は，有限要素法を用いた 2 次元逆解析を用いた．その結果，深度 1000 m までの比抵抗構造が得られた．クッタラカルデラの下には，鉛直方向に伸長する低比抵抗領域（＜30 Ω·m，深度 1000 m 以上，東西径 1300–1500 m）が存在し，この領域はカルデラ形成により落ち込んだ溶岩ブロックや火山砕屑物等が熱水変質を受けたものであると推定される．この低比抵抗領域は，クッタラ湖の中心からやや東に位置する湖盆地形の直下にあり，カルデラ陥没は主にこの地点で行われたと考えられる．カルデラの西部は地滑り等により拡大された可能性が高い．クッタラカルデラの内部構造は東西非対称であり，非対称なカルデラ陥没はクッタラ火山の非対称な地質に起因すると考えられる．